Università degli Studi di Padova
Dipartimento di Fisica ed Astronomia "Galileo Galilei"
Corso di Studi in Fisica

Analysis of the diagnostic potential of a wire calorimeter for characterization of particle beams

Relatore: dott. Gianluigi Serianni
Correlatore: dott. Roberto Pasqualotto

Laureando: Marco Zanini
1029500

Anno Accademico 2013/2014

Ai miei genitori
A Marta
A Margherita

Abstract

To optimise the particle beam for the nuclear fusion experiment ITER it is necessary to measure the beam parameters with high spatial resolution. This can be done with a diagnostic calorimeter composed by an arrangement of wires made of suitable material. The wires heat up because of the deposition of power due to the particle beam and reach a temperature high enough to irradiate the thermal power received. The present thesis proposes the design of an experiment to calibrate a wire prototype, using ohmic heating to heat the wire observed with a visible camera. A numerical computation is also performed to simulate the results of the ELISE particle beam, operating at Max-Planck Institut für Plasmaphysik,in Garching bei München.

Contents

1 Introduction

1.1 ITER

After the discovery of the nuclear structures of atoms, two new ways for the energy production were conceived: nuclear fission and nuclear fusion.

The first is nowadays largely widespread and it is based on the splitting of heavy nuclei (generally Uranium) into lighter nuclei, but the production of a large quantity of radioactive waste that must be stored for thousands years represents a limit for this technology.

The energy production with fossil fuels is no longer sustainable because of the excessive pollution and the continous decrease of reserve while renewable sources can not sustain alone the energy needs.

A solution can be offered by nuclear fusion: it is used as weapon since 1952 but the realisation of a nuclear reactor is still incomplete. In theory, two light nuclei can be bound together due to Strong Interaction to create a heavier nucleus and the binding energies are equal to the produced energy. However, the Coulomb interaction between the nuclei is very strong and particles need to have high kinetic energy to get close enough that the Strong Interaction plays a large role. A little probability to overcome the potential barrier exists due to Tunnel Effect. In particular, the statistical fluctations of the Maxwell-Boltzmann function and the quantum-mechanical effects allow the fusion of the nuclei, even if average kinetic energy is lower than the energy of the potential barrier.

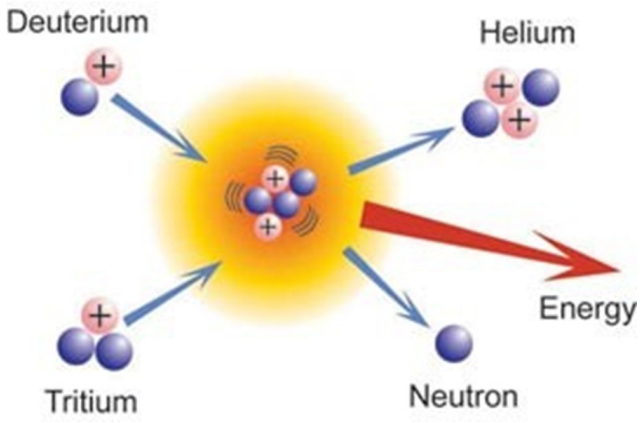

Figure 1: D-T reaction

Several exothermic nuclear fusion reactions are known; the most probable process consists of deuterium-tritium (D-T) reaction because it has the bigger cross section with respect to other fusion reactions of light nuclei. The energy production is equal to the binding energy:

$$D + T \rightarrow^4 He + n + 17.6MeV \tag{1}$$

Deuterium is aviable in water, while tritium is not a stable isotope: its lifetime is about 12 years. To satisfy the tritium requirements, lithium can be used, as described in the following reactions:

$$n +^6 Li \rightarrow^3 H +^4 He \tag{2}$$

$$n +^7 Li \rightarrow^3 H +^4 He + n \tag{3}$$

The maximum of the cross-section, and so the probability of collisions, for those reagents is at a temperature around 100keV, as can be seen in figure 2, and this energy has to be supplied to the particles.

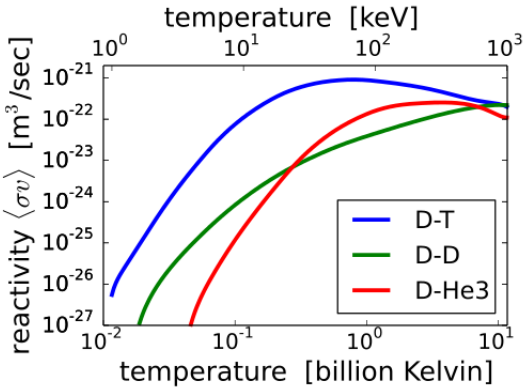

Figure 2: D-T reaction

Two artificial techniques have been developed to obtain controlled fusion reactions. On Earth the first one exploits the inertial confinement: high intensity LASER pulses compress atoms and the nuclei can overcome the Coulomb barrier. This kind of project is carried on for istance in USA with the National Ignition Facility.

The second way applies a suitable magnetic configuration. At the high energies required for fusion reactions to occur, matter is in the state of plasma, whic represents the fourth state of matter: electrons and nuclei are not bound together and it can be described as a locally charged fluid. Magnetic confinement is fundamental to reduce plasma losses and the contamination with impurities originated by the plasma-wall interaction. Moreover, it reduces collisions with the machine. Charged particles in the plasma will follow magnetic field lines, generally in a toroidal shaped structure, and a net electric current is generated. Several configurations are studied, but the TOKAMAK yields at present an higher temperature than the other configurations. The toroidal magnetic field, produced by superconductive magnets, is superposed with a poloidal field, created by the toroidal current generated by the variation of current in the central solenoid, placed on the axis of symmetry fo the torus[1].

Moreover, this current also heats the plasma due to ohmic heating. This field is necessary because a purely toroidal magnetic field would yield a strong particle drifts, perpendicular to the magnetic field lines, that reduce particle confinement effects.

Thermonuclear reactors present many advantages with respect to nuclear fission reactors.

- Radioactive wastes are composed by structural materials, activated by the neutron flux. They possess a shorter lifetime than fission wastes.
- Deuterium and Lithium are widespread on Earth's crust and oceans, while Uranium reserves are limited.
- Fusion reaction is intrinsecally safe as it is not self-sustained. To achieve and sustain it, hard physical conditions have to be achieved and it can be easily shutdown in case of accident.

The ITER (the latin word for "the path") project has been estabilished to demonstrate the feasibility of thermonuclear fusion as an electric energy source, with a TOKAMAK configuration, using D-T reaction.

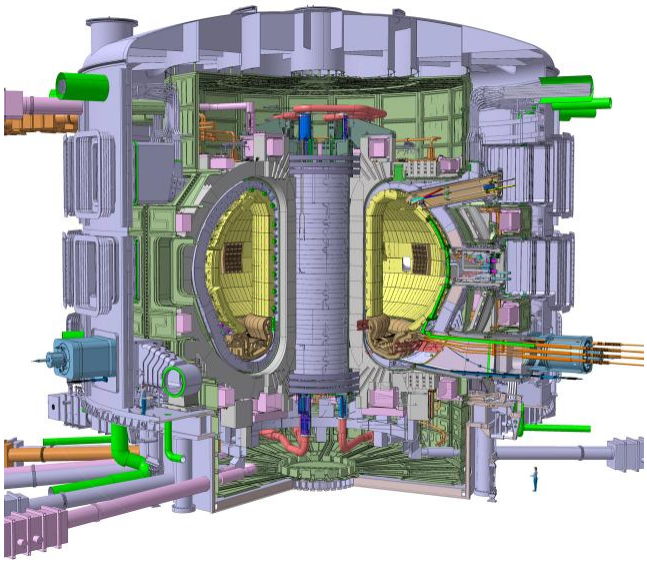

Figure 3: ITER Tokamak. The person on the right gives an idea about the reactor size. ITER Tokamak chamber will be twice as large as any previous tokamak, with a plasma volume of 830 cubic metres. [2]

The first aim of the this project is to obtain an energy gain factor Q, such that $5 < Q < 10$ in stationary conditions.

The energy produced in the reaction, equation 1, is the kinetic energy of the fusion products: $3.6MeV$ for Helium and $14.1MeV$ for neutrons that have no electric charge and so they pass through the magnetic field until they collide with the blanket. The experiment requires proper materials like Beryllium for the first wall, to reduce the losses due to impurity line radiation while the rest will be constituted of high-strength

copper and stainless steel, to make it resistant to mechanical stresses and to shield the vessel and supercunductive materials from the neutron flux. Here, neutrons are absorbed by walls and their energy is turned into heat. [2]

In an industrial power plant, this energy will be next converted in electric energy.

In a later experimental phase, prototype breeding modules will be used to test materials for *"Tritium Breeding"*. Infact,it is not possible to conply externally with to the complete tritium requirements and it is necessary that the TOKAMAK produces it, making the escaping neutrons interact with Litium nuclei contained in the blanket, as described by reactions 2 and 3.

To turn the gas into a plasma and to reach the threshold temperature that allows D-T reactions, an external heating system is required and several methods have been studied as the ohmic heating is not sufficient: plasma can be considered as a conductor material and because of the magnetic fields used to control it, high-intensity currents are generated and their flowing have heating effect.

However, as the temperature rises, plasma resistance (and the heating effect) decreases [3] and other heating methods have to been used to reach the required energy level that makes fusion possible; in the ITER Tokamak, ohmic heating will be supplemented by high-frequency waves and neutral beam injection.

Electromagnetic waves will be generated outside the TOKAMAK and propagating them inside the plasma, waves energy shall be released to the charged particles. In particular, two different resonance frequencies will be used to heat ITER plasma:

- Ion cyclotron frequency $\omega = \frac{eB}{m_i}$
- Electron cyclotron resonance $\omega = \frac{eB}{m_e}$

1.2 Beam Injection System

Another plasma heating method is based on the injection of high-energy nuclei (hydrogen and deuterium in ITER) inside the confined plasma. To reach plasma core, these nuclei have to be neutral not to be deflexed by the magnetic field. ITER will be equipped with two neutral beam heating and current drive injectors: each one delivering a deuterium beam of 16.5 MW with particle energies of $1MeV$, and able to operate for long pulses up to $3600s$[4].

Hydrogen and deuterium ions are created in a plasma and an extraction/accelerator system accelerates them to the required energy. Accelerated particles pass through a gas cell where about 60 % is neutralized via collisions. Residual charged particles are collected by the Residual Ion Dump that deflects them with a magnetic or an electric field and prevents them from reaching the edge region of the TOKAMAK plasma where the magnetic field would deflect them onto material surfaces.

Neutralisation process efficiency is different for positive o negative ions. Some studies show that negative beams have a neutralisation efficiency about 60% even at higher energies, while positive ion efficiency tends to become zero[1]. For these considerations, ITER beams will use H^- and D^-. The source of the injector will be a RF driven negative ion source, developed and studied at IPP[6]. In sources of these type, RF coil induces oscillating electric field that accelerates electrons in the source body and generates a plasma by ionisation.

The edge between the plasma and the region in which charged particles feel the interaction with the electric field of the grid is called *"meniscus"*. It is defined as the region with potential equal to zero with respect to the source and it has the shape of a convex lens. Grids are used for the acceleration system and each one has several apertures. Particles that pass through an aperture form a beamlet and the beam is composed of several beamlets (1280 for ITER injector). Optical properties of each beamlet depend on the space charge distribution and, moreover, on the electric and magnetic fields of the extraction/acceleration system. The maximum current that can be extracted is limited by *Child-Langmuir Law*[5]:

$$I_{ex}^{max} = \frac{4}{9}\pi\epsilon_0 \cdot\sqrt{\frac{2e}{m}}\left(\frac{r}{d}\right)^2 V_{ex}^{\frac{3}{2}} \tag{4}$$

Defining:

$$\Pi = \frac{I_{ex}}{V^{\frac{3}{2}}} \tag{5}$$

Π is named perveance and

$$\Pi_0 = \frac{I_{ex}^{max}}{V_{ex}^{\frac{3}{2}}} = \frac{4}{9}\pi\epsilon_0 \cdot\sqrt{\frac{2e}{m}}\left(\frac{r}{d}\right) \tag{6}$$

where r is the aperture radius and d the distance between the plasma grid and the extraction grid.

Perveance Π is a fundamental parameter used to describe beam optics. Normalized perveance, defined as $\frac{\Pi}{\Pi_0}$, is used to describe beam optics due to its relation with the beam divergence, index of the beamlet opening caused by charge expansion. Generally, divergence ϵ depends on the perveance and on the ratio between extraction and acceleration voltage. The increment of $\frac{\Pi}{\Pi_0}$ yields a decreases of the divergence until it reaches its minimum value. After this value, it increase again. This minimum divergence value gives the optimal perveance.

Since the main parameters of ITER neutral beam injector, total current, particle energy and pulse duration, have never been attained simultaneously, PRIMA [7] test facility has been commissioned and actually is under construction at Consorzio RFX,

in Padova. It will include two experimental devices: a full size plasma source with low voltage extraction, named SPIDER[8] and a full size NBI with a full beam power corresponding to $1MV$, named MITICA. The main requirement for the full sizze ion source is to demonstrate the capability to produce high negative ion current density.

Here a representation of the injector:

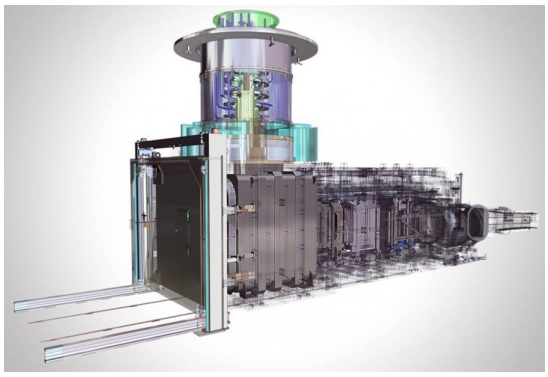

Figure 4: NBI

1.3 ELISE test facility

Another test facility, ELISE[9], has been designed and installed, in 2009, at Garching bei München IPP. This negative hydrogen ion source investigates a source half as large as the future ITER source.

ELISE produces plasma up to 1h, accelerates a negative ion beam (H^- or D^-) up to 60kV for 10s, every 180s via an ITER-like extraction system. It is designed to extract a current of 20A using a three-grid extraction system that consists of 640 extraction apertures (with a 14mm diameter for the plasma grid) arranged in a 2 $\times$ 4 beamlet groups. Each one of this is formed with 5 $\times$ 16 apertures, spaced 20mm $\times$ 20mm. The accelerated beam is stopped on a calorimeter.

1.3.1 Diagnostic Tools in ELISE

ELISE is equipped with several beam diagnostic tools [11] (figure 6) to obtain information about beam parameters, such as position, divergence, profile, intensity, homogeneity and stripping losses. The beam physics requires the measurement of the beam parameters with an high spatial resolution and in ELISE this is made with different techniques. It was initially equipped with a beam dump for a faster ion source commissioning, while in a second experimental phase, beam analysis will be made with a diagnostic calorimeter, a tungsten wire calorimeter and a H_α Doppler shift beam spectroscopy.

- The beam dump consists of 4 HCP(High Conductivity Phosphorus grade) copper plates, 2 cm thick, covering a total area of $1.2mm \times 1.2mm$. It is designed to

stop an ion beam of $20A$ and $2°$ of divergence. Plates are inertially cooled: their temperature increases during pulses and it is cooled down to room temperature during the pauses. Moreover, a water calorimetry will provide to measure the total beam power, averaged over $10s$

- A diagnostic calorimeter has been installed, at the end of 2012, to provide more information about beam profile and its homogeneity. It is constituted of 4 HCP copper plates, each one $0.6m \times 0.6m$. Also for this diagnostic tool a water calorimetry provides an indipendent measurement of the beam total power for all the four copper plates. Moreover, each plate temperature is measured by 12 thermocouples.

- H_α Doppler shift beam spectroscopy provides the quantitative characterization of: beam divergence and stripping losses. This spectroscopy has a spatial resolution of 20 channels: 16 vertically-arranged lines-of-sight (LOS) and 4 horizontally-arranged LOS. The collected light is transmitted by optical fibers through a feedthrough and then it is analyzed using an Acton Spectrometer with a focal length of $0.75m$. Analysis of width of the Doppler shifted H_α peak provides LOS-averaged beam divergence.

- A W-wire calorimeter[10] (figure 5) was placed perpendicularly to the beam at 1.8m of distance from the grid of acceleration and it will be composed of a two-dimensional arrangement of 100 tungsten wires spaced by 20mm. The wires lie in two vertical planes, distanced 10mm, in which wires are disposed horizontally and vertically. The ion beam heats the wires up to 2600K and thermal equilibrium is reached in 1s. Because of the thermal expansion, the wires expand several mm so it is necessary to keep them under tension through wire holders. Emitted light is observed with an optical CCD camera positioned on the front surface mirror. With this kind of calorimeter it is possible to obtain fast qualitative data about the image of beam position.

In figure 5 ELISE tungsten wire can be seen. The three images show how the global beam varies changing the voltage. All information about ELISE diagnostic has been taken from [12].

Figure 5: ELISE W-Wire calorimeter

Diagnostic tools of ELISE are visible in figure 6.

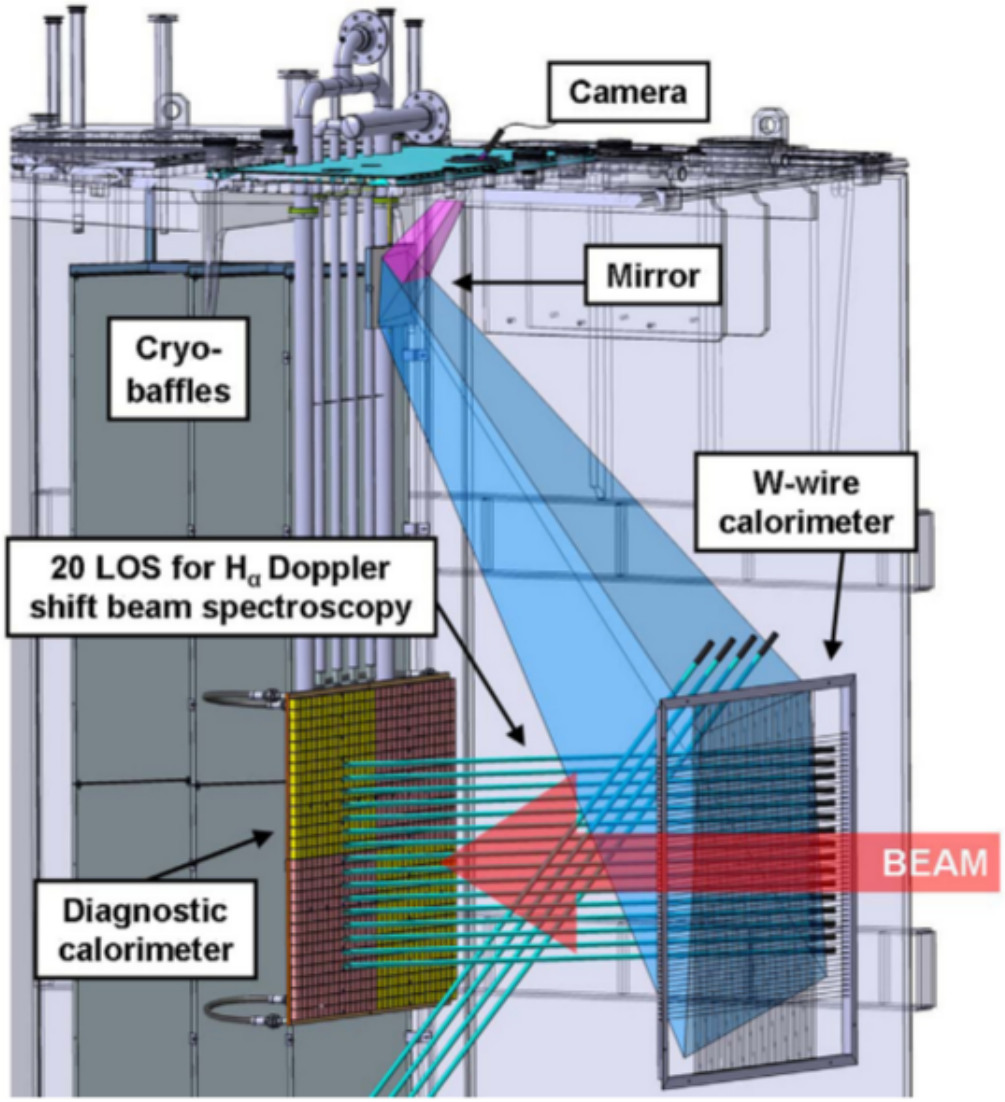

Figure 6: Diagnostic system for ELISE beam properties

2 Expected behaviour of tungsten filaments

The knowledge of tungsten filaments behaviour is fundamental to organize the experiment and to analyze collected data. In the first section attention will be paid to the radiation emission of heated bodies, while in the second electrothermal effects will be discussed.

2.1 Black Body Radiation

Continously, any body emits electromagnetic radiations, in all wavelengths. Near the equilibrium, the radiation is well described by Planck's Law and it has a maximum intensity at a specific wavelength that depends only on the temperature. In particular, it is found that hte higher the temperature,the lower the wavelength of the intensity maximum, as in the following graph:

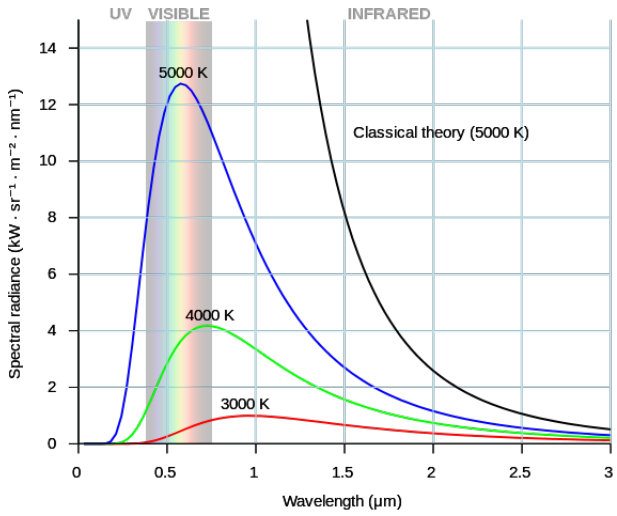

Figure 7: Black Body emission spectra

The intensity distribution of the black body radiation with temperature T is given by Planck's Law (that can be exposed in two ways):

$$B(\nu)d\nu = \frac{2h\nu^3}{c^2}\frac{1}{e^{\frac{h\nu}{kT}}-1}d\nu \tag{7}$$

or

$$B(\lambda)d\lambda = \frac{2hc^2}{\lambda^5}\frac{1}{e^{\frac{hc}{kT\lambda}}-1}d\lambda \tag{8}$$

By these equations, the derivation of the Stefan-Boltzmann Law is possible and after some calculations, the total power emitted by heated body can be written as:

$$P_{irr} = \epsilon \sigma S T^4 \tag{9}$$

where ϵ is the emittivity, σ is the Stefan-Boltzmann constant and S the surface of the body. The black body represents the ideal case and the emissivity is equal to 1: in that way, it emits all the input power. In reality the emissivity tends to be lower and these bodies are named grey body. The literature evidences several different emissivity behaviours.

In part of the experimental experimental sessions described in this thesis a spectrometer has been used to collect the emission spectra of the filament. It shall be described in section 3.2, while the analysis data shall be shown in section 3.3.2.

In [14] it is reported that metal oxides show a little variation in emissivity with temperture, but the same thing is not true for pure tungsten: in this case it varies with temperature: authors found a linear dependance in filaments of incandescent lamps that yields $I \propto T^5$. The same effect is not present in filament radiators whose surface is oxidized and the emissivity remains a constant. In another article [13] some works are quoted: the first support the thesis about the independece from temperature for oxidized filament surfaces. On the other hand, in other quotations it is reported that if filaments have a bright metal surface, a linearity between the emissivity and the temperature is found. Neverthless, the same author concludes that "the problem remains unsolved".

The article continues with some analysis to calculate the value of the temperature exponent which is found to be very close to 4, in accordance with equation 9.

Other papers ([15] and [16] show the emissivity as a function of the temperature, but the relationship is not linear.

From these articles, it can be concluded that tungsten emissivity behaviour is not completely clear and these former references can not be taken into consideration during the analysis. A dedicated analysis was performed to asses the dependence of the emissivity on temperature in this experimental case.

2.2 Electrothermal Behaviour

If an electric current I flows in a body, the electric power $P = VI$, where V is the voltage drop across the body, is turned into thermal energy and the body temperature rises; incidentally that causes thermal expansion. Moreover, electric resistance is not a constant, but strongly depends on temperature. In a conductor, this dependence can be linearized as [18]:

$$R(T) = R_0[1 + \alpha(T - T_0)] \tag{10}$$

where α is a constant (for tungsten, $\alpha = 0.0053K^{-1}$)

In some article [14] another trend is demonstred for a tungsten filament:

$$R(T) = R_0[1 + 5.238t + 0.7t^2 + 0.062t^3] \tag{11}$$

with $t = (T - 273)/1000$ and R_0 is the resistance at 273 K.

An estimation of filament temperature can be obtained from the computation of electrical resistance:

$$T = \left[\frac{V\pi r^2}{Il\rho_0} - 1\right]\frac{1}{\alpha} + T_0 \tag{12}$$

where l is the length of the filament, r is the radius, ρ tungsten resistivity at room temperature. In this formula the filaments are assumed to be homogeneously heated. Its limitation will be discusses in section3.3

3 Analysis of the potentiality of a W-Wire Calorimeter

This work aims to demonstrate the possibility of using a W-wire calorimeter not only to have qualitative information about beam position, but also to obtain other information, such as the deposited power on the filament to make possible a determination of the beam energy flux.

This can be done by showing the existence of a monotonic relationship between the emitted light and the deposited power on the filaments. In the first part of this section the preparation of the experiment devoted to asses this relationship will be presented; in the second section it will be described how data have been collected while in the third section analysis results will be exposed.

3.1 Development of the experiment

With reference to figure 8 filaments have been placed in a vacuum chamber with four apertures. One of these has been used as base and another one was closed with a glass and the CCD[19] camera was attached to its flange to be perpendicular to the filament. The whole system in shown in figure 10 For the latest tests a spectrometer has been added to measure emission sprectra. CCD and the specrometer fibre holder are visible in Figure 9 and in Figure 13b.

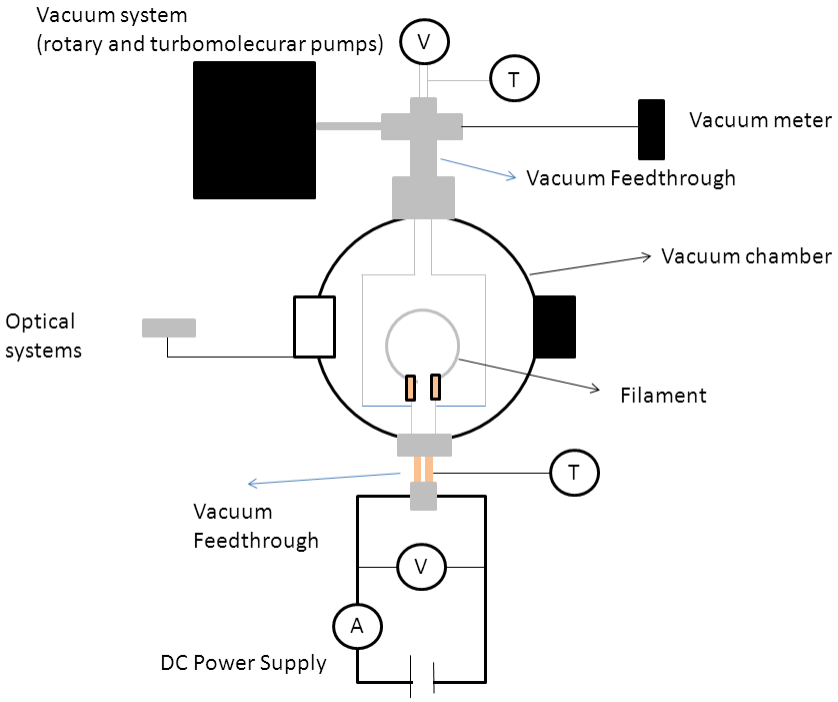

Figure 8: Experimental device scheme

.

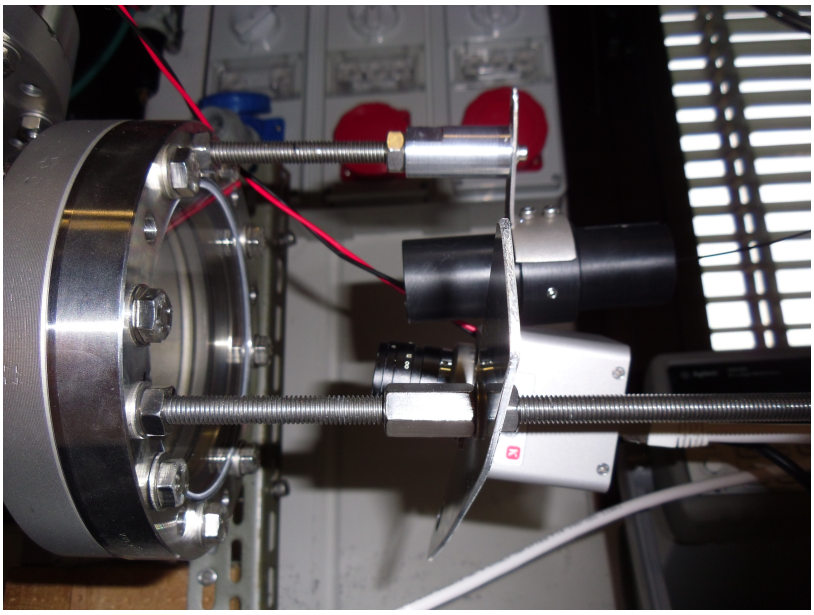

Figure 9: CCD camera and Spectrometer

The camera has been placed at the minimum distance that allows focusing onto the wire. It collects radiation from $350nm$ to $1150nm$, each wavelengths with a certain quantum efficiency, and the glass (KODIAN 7056) has been selected so as to be transparent for these wavelength.

The spectrometer collects radiation from $300nm$ to $800nm$ and due to the high filament brightness it was necessary introducing a filter with an attenuation factor equal to 10^3. Collected spectra has to be recalibrated and this will discussed in section 3.3.3. Due to the following calibrations are only power-based, the spectrometer was not fundamental at this scope, but it has been used to obtain further information about filament temperature and spectrum.

A direct current generator (EUTRON BVR2000 40V 45A) is connected to the wire through a vacuum feedthrough; the electrode temperature was monitored by thermocouple to keep it under the safety threshold (about 80°).

The creation of a support to connect filaments with the vacuum feedthrough was necessary; these copper blocks have been designed during the present thesis (figure 11) to permit their insertion in the feedthrough electrode and they have been completely built at Consorzio RFX workshop. The volume of the chamber and the cross-section of the aperture have been taken into consideration during the design to place the central part of the tungsten wire in the centre of the CCD frame. Moreover, due to their dimension ($15mm \times 15mm \times 30mm$), these connections give a negligible contribution to the total electric resistance. Parallelepiped shape has been preferred for the copper block to make the realisation easier. Holes on the side allow the insertion of the filament, long about 0.22m, which is then brazed to the copper block, and the total support is

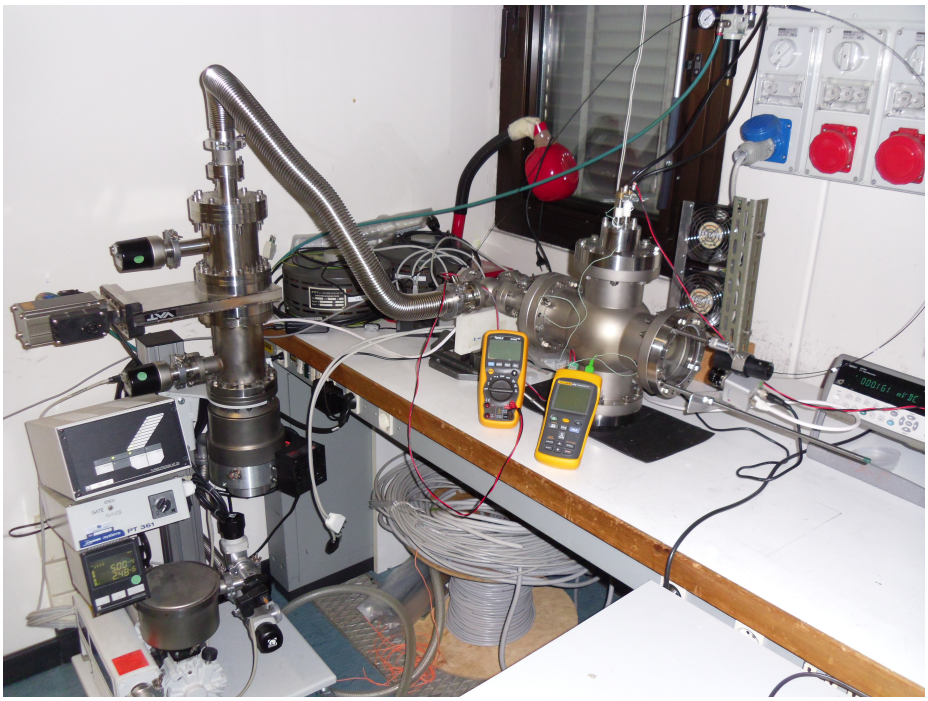

Figure 10: Experimental apparatus

about $90mm$ long and $80mm$ wide, as can be seen in figure 13a

Holes were drilled to insert a thermocouple and two electrical wires that pass through the fourth aperture in which another "cross" is present. This allows the connection to vacuum pump and vacuummeter. Copper blocks before brazing are visible in figure 12a, while filament brazed are shown in 12b.

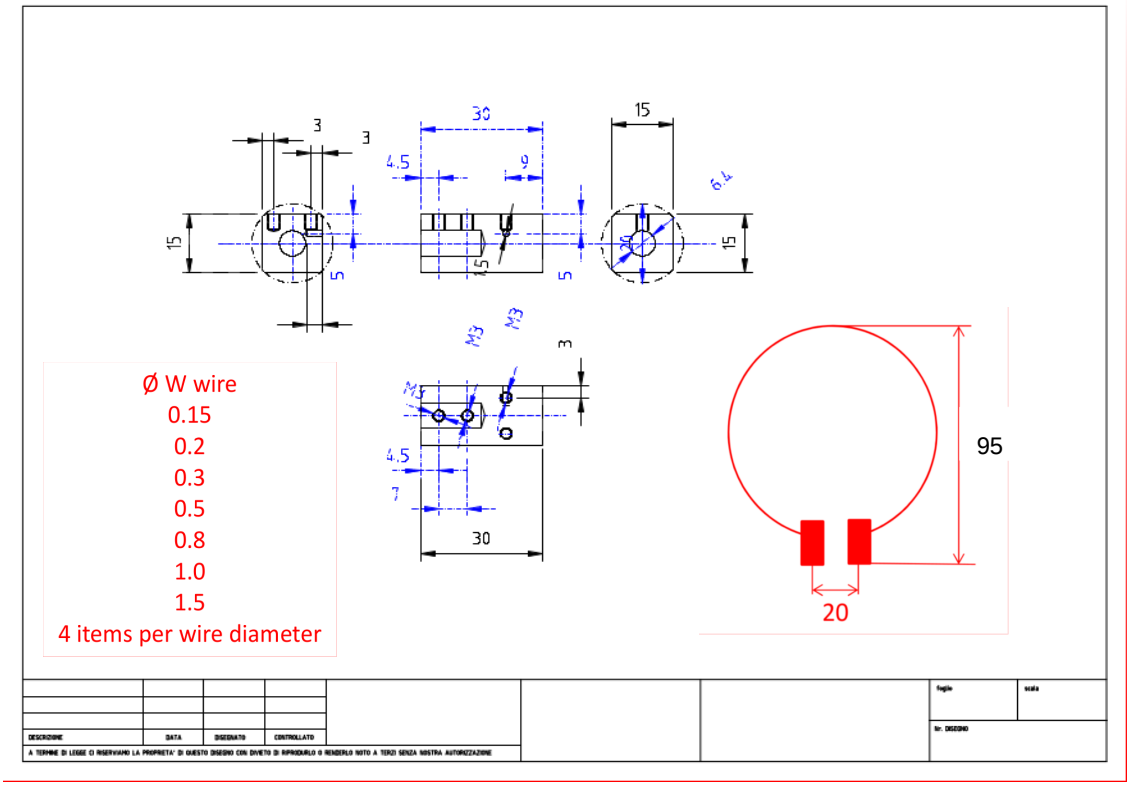

Figure 11: The original support CAD project

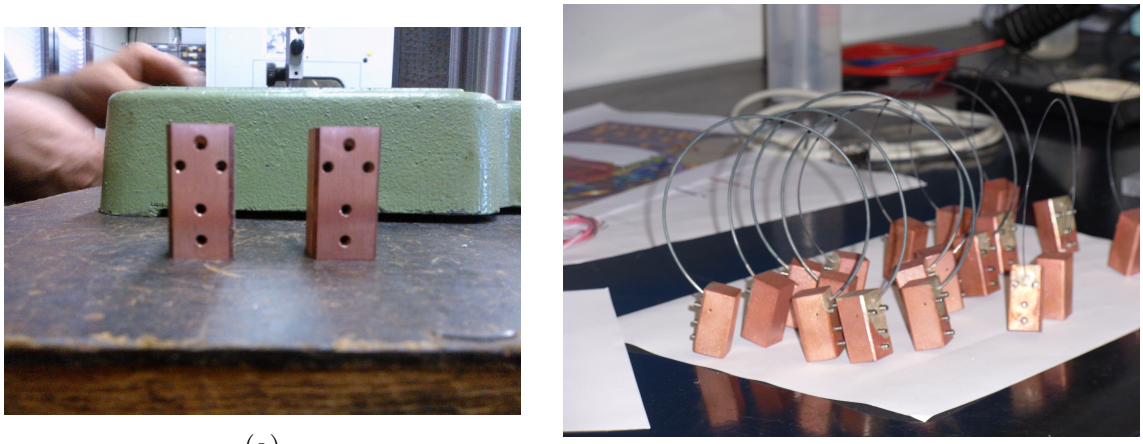

(a) (b)

Figure 12: Filament supports

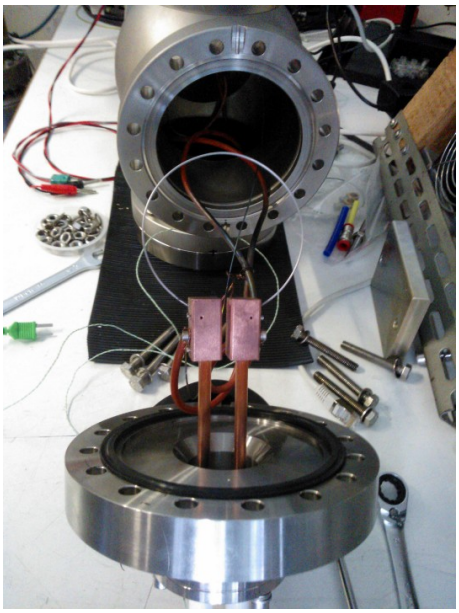

(a) Support connected to the vacuum feedthrough

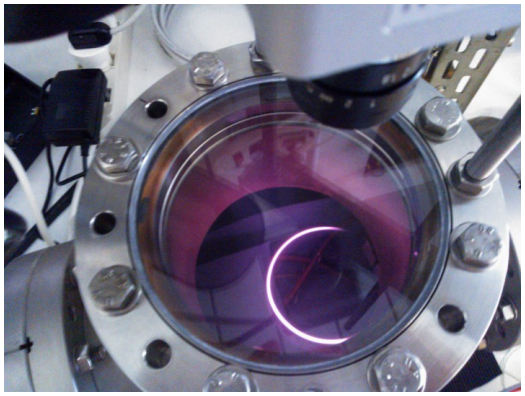

(b) Heated Filament

Figure 13: Filament in vacuum chamber

3.2 Experimental data

The aim of the measurements is to find a correspondency between the radiation collected by the camera. Tungsten filaments have been heated via ohmic dissipation (figure 13b). The total power supplied is $P_{in} = VI$ and in accordance with energy conservation, filamentents emit this power, dissipating it into the environment by radiation and conduction, as in the following equation:

$$VI = P_{in} = P_{out} = \epsilon S\sigma(T^4 - T_0^4) + k(T - T_0) \tag{13}$$

the first term has been already discussed in section 2.1, while the second represents conduction effects. Since the filament calibrations need only the collected light, the second term can be neglected in following calibration analysis.

Moreover, this phenomenon has been extensively discussed in [17], where it is found that it can be neglected for thinnest filaments of those reported in table 2.

Collected Light (a.u.) is the portion of the total emission spectra that can be collected by the CCD camera. Infact, due to the limitation of CCD and spectrometer, not all the spectrum radiation can be observed.

It has been discussed in section 2.1 (equation 8) that the maximum moves to the left and so the collected radiation not only increases due to the temperature increment, but also due to the bigger portion of the curve in the wavelength interval, as can be seen in table 1. For example, at about 2350 K only 18% of the total light emission is

$T(K)$	2352.52	2303.08	2219.14	2103.12	2007.76
%	18	16.9	14.9	12.3	10.2

Table 1: Percentual ratio

in the wavelengths range of camera as at these temperatures the peak of the curve and the biggest part of the radiation correspond to higher λ than collected λ.

Computing these areas in the delimited region and dividing them for the areas in the complete spectrum, the contribution of this effect can be quantified. In partic3.1.2ular, this increase will surely give a contribution to the temperature dependancy.

Several filaments with different diameters have been tested, sometimes several times. Those are reported in table 2.

number of filament	campaign	diameter	number of scans	use of spectrometer
1	20140716_0.8mm	0.80mm	1	no
2	20140718_0.8mm	0.80mm	1	no
3	20140718_1.00mm	1.00mm	1	no
3	20140721_1.00mm	1.00mm	1	no
4	20140722_0.5mm	0.50mm	3	no
5	20140724_0.5mm	0.50mm	1	yes
6	20140724_0.3mm	0.30mm	1	no
7	20140829_0.3mm	0.30mm	4	yes
8	20140904_0.2mm	0.20mm	3	yes

Table 2: Number of the filament, name of the experimental campaign, filament diameter and number of scans. For the 5^{th} filament the spectrometer has been used, but all measurements saturated. These will not be presented.

Current has been slowly increased, generally every $0.5A$ and for each amperometric step the following data have been collected, not only for the data analysis, but also to control temperatures of supports and electrodes:

- temperature of the copper blocks (thermocouple "Type K")
- temperature of the feedthrough electrodes (thermocouple "Type N")
- current as indicated by the power supply display
- current as indicated by the current clamp (LEM LH2015)
- voltage drop between the feedthrough electrodes (Multimeter AGILENT 34410A)
- voltage drop between copper blocks (NIMEX NI 4600)

- pressure (Leybold PTR90 and Leybold TERMOVAK TTR 91)

Moreover, at least one filament image was taken: until the filaments emit no electromagnetic radiation only one image was taken. When the filament was emitting light generally three images, with different integration time, were recorded, as can be seen in Figure 14a and 14b .

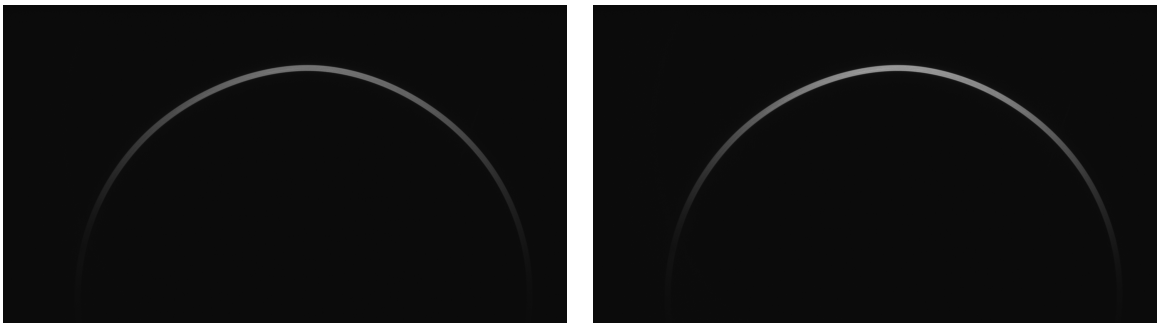

(a) Image with 75ns (b) Image with 100ns

Figure 14: Images with different integration time

The incident photons on the CCD generate electrons, due to photoelectric effect, that are stored and the result is a signal proportional to their quantity. The camera used in the experiment has a saturation level equal to 255. When this level is reached, the electronic system can not store more electrons and the proportionality between the signal and the incident photons is not more guaranteed. The integration time is the exposure time of the CCD to radiations: the longer the integration time is elevated, the more photons produce electrons that will be converted into signal. Integration time was selected as high as possible, to reduce the influence of background effects.

In the experiment the linearity between signal and integration time is fundamental and it was verified.[17]

Images have been analyzed with a ROOT macro that normalizes pixels to their integration time to obtain the trend of the radiation emission as a function of input power. To have better information about how this macro works, see [17]. In particular, it has to be seen in Figures 14a and 14b that filament heating is inhomogeneous and because of it each infinitesimal section gives a different contribution to total electric resistance. Moreover, as it can be seen, the closer the sections to the support, the colder they are. Due to this effect, nominal length can not be used to deduce the temperature of the brightest part of the filament, but the definition of an effective value has to be done. Some estimations will be done in section 3.3.3, using temperature values obtained by indipendent method.

3.3 Data Analysis

The present section describes data analysis and is composed of three parts. The first aims to verify the reproducibility of electric measurement; only graphs will be presented. In the second part, filament calibrations will be discussed, while in the third part the introduction of the spectrometer will yield an estimation of the temperature and the effective length of the wire.

3.3.1 Reproducibility of I-R curve

The first thing is the demonstration of reproducibility. This has been quite well verified, except for the first data collection of each filament. Infact, as can be seen in figures 15 and 16,in the first session, when current was gradually increased, a discontinuity is visible. It has been verified that this phenomenon is present for each filament and it happens at the same estimated temperature, about 1300 K; it is probably caused by expulsion of impurities from tungsten so that its properties are modified. During this process filaments temperature suddenly increases causing also an increment of the emitted radiation and electric resistance, in accordance with equation 10. In the second session, the current has been decreased but this effect did not happen; also in third session, in which the current has been increased again, there is no discontinuity.

As an example, all data can be seen in figure 16 for the wire 4), with a $d = 0.5mm$: in particular it has to been noted that the curve of the first session (in red) have a different trend, while the second part is overlapped tp the other curves.

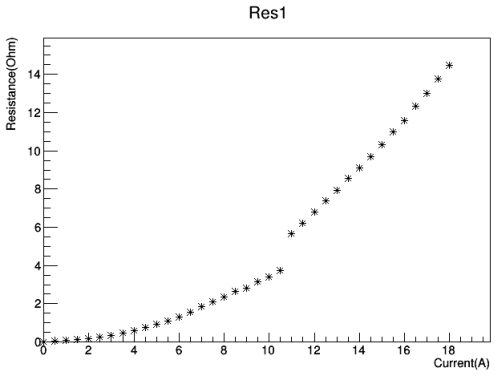

(a) First session

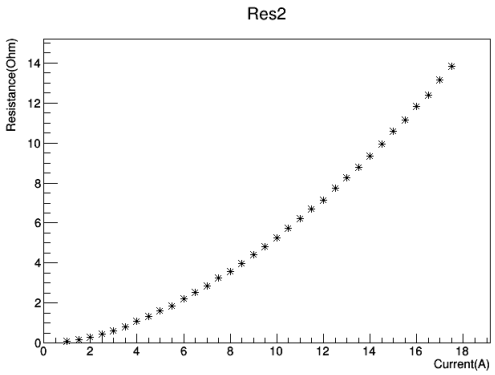

(b) Second session

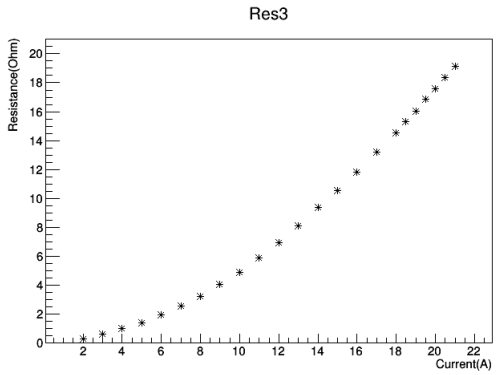

(c) Third session

Figure 15: I-R plots of filament 4), $d = 0.5mm$

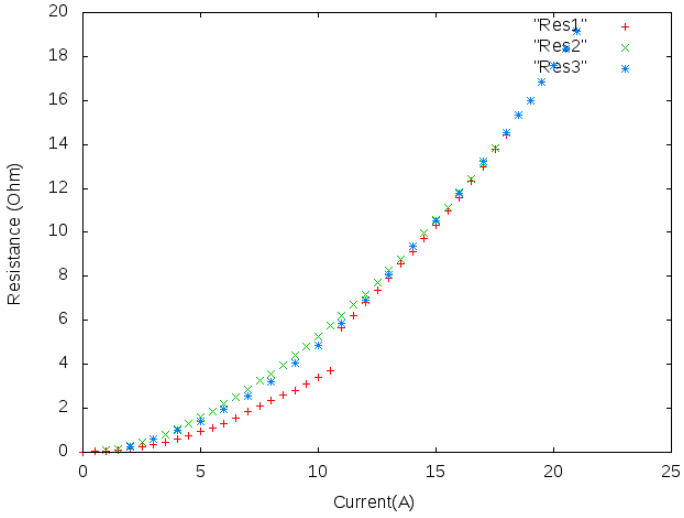

Figure 16: Overlap of (I,R curves of the same filament)

3.3.2 CCD Camera

Initially, analysis was based on (T,P_{coll}), using T estimated by equation 12. Obtained trend have been confronted with theoretical one. To compute it, Planck equation, properly convoluted with quantum efficiency of the CCD[1], has been integrated in the wavelength interval, using the same temperatures of the plot.

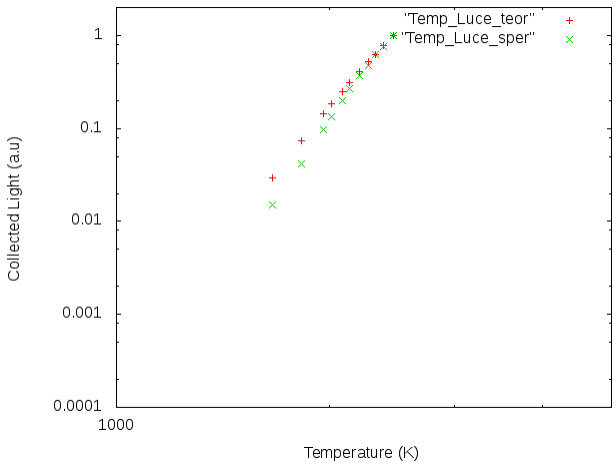

Figure 17: Bilogarithmic graph of (T,P_{coll}) in green and (T,Theoretical emission)in red.

As can be seen in graph 17,the two curves present a big difference and no explanation has been found. Moreover, temperature has been calculated using equation 12, in which homogeneous heating is assumed. As it has been said at the end of section 3.1,filaments tend to be hotter in centre and colder in part closed to the copper support.

Instead of the length of the filament an effective one (l^*) should be used and this consideration makes equation 12 unreliable without a proper value for l^*. Due to the necessity of a better temperature calculation, it has been decided to use a spectrometer. Moreover, the following calibration analysis will be based on (VI,P_{coll}) to avoid inaccurate data on x-axis.

P_{coll} (a.u.) is proportional to the emitted power and plot the provides the calibration of the filaments. As can be seen in figure 18, for very different wire diameter, data are monotonic, which anyway allows meaningful calibration.

These data represent Power-P_{coll} plots of two filaments with a different diameter. In the first case current has been slowly increased up to $45.7V$, while in the second current has been initially increased and then decreased. Collected Light, P_{coll} (a.u.) data has been divided by their maximum value to obtain only relative data since the most important parameter in following fit is the trend. The monotonicity has been verified in all experimental sets and this make filament calibrations possible.

A suitable function to fit Power-P_{coll} was sought for:a function such as $y = ax^b+c$ was chosen. All data have been fitted according to this model; data with the discontinuity

[1]Quantum efficiency CCD camera is described at [19]

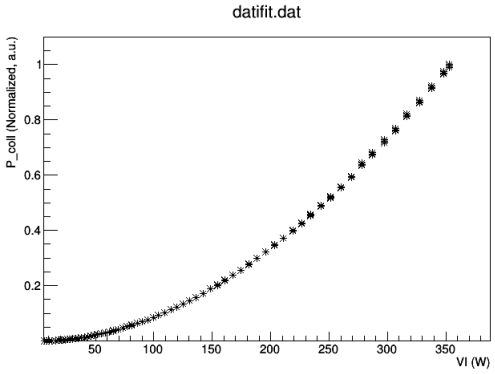

(a) Linear scale, diameter = 1mm

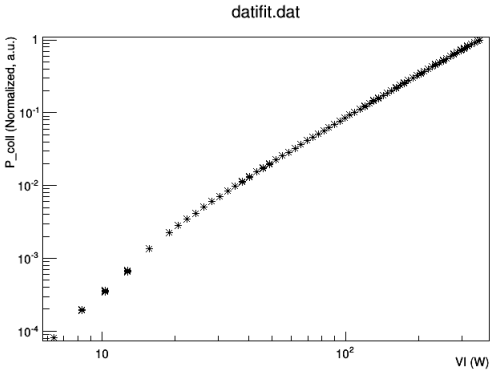

(b) Bilogarithmic scale, diameter = 1mm

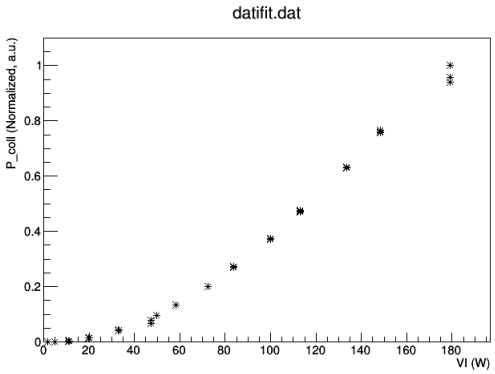

(c) Linear scale, diameter = 0.2mm

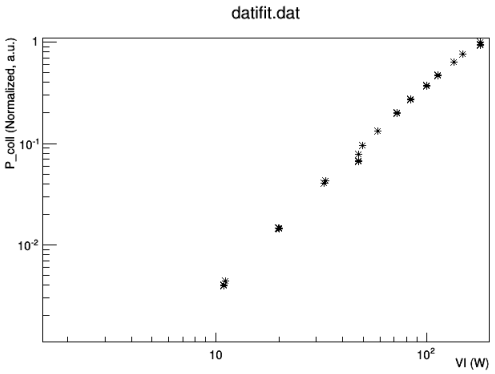

(d) Bilogarithmic scale, diameter = 0.2mm

Figure 18: Power-P_{coll} plots in linear and bilogarithmic scale of 2 filaments with different diameter

have been discarded because they were no reproducible and so they yield no useful information to calibrations. Data and fitting functions are shown in figure 19:

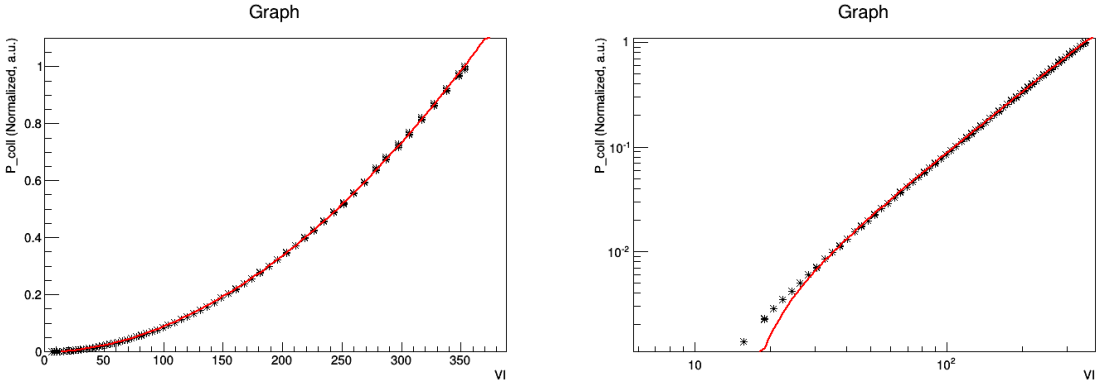

(a) Linear Scale (b) Bilogarithmic Scale

Figure 19: Power - P_{coll} fit

All fit resuls are shown in table 3

Nome scansione	a	b	$c(nm)$	σ_a	σ_b	$\sigma_c(nm)$
20140721_1.0	1.32E-005	1.916	-2.55E-003	2.83E-007	3.71E-003	3.60E-004
20140722_0.5	9.33E-006	1.936	4.15E-003	3.86E-008	2.71E-009	1.12E-003
20140724_0.5	3.31E-005	1.902	-2.07E-003	1.79E-006	1.02E-002	7.35E-004
20140724_0.3	5.09E-005	1.981	-1.30E-002	1.36E-005	5.38E-002	4.25E-003
20140829_0.3	3.73E-005	1.929	5.29E-004	1.05E-007	7.61E-009	1.13E-003
20140904_0.2	1.78E-004	1.667	-1.14E-002	3.33E-005	3.66E-002	4.32E-003

Table 3: Fit results

As can be seen in Table 3, all fits present similar exponent parameters. It has to been noted that P_{in} and P_{coll} have not a linear relation. This has already been discussed in table 1, section 3.2; the hotter the filaments, the larger the shift of the Planck curves towards lower wavelengths and so the bigger the collected portion of the emitted radiation. This surely gives a contribution to the value of b.

To complete the calibration, a conversion between electric power and beam power must be done: when the calorimeter will be hit by the particle beam, it will emit electromagnetic radiation. This value has to be confronted with the calibration curve and the corresponding power can be determined. Infact, with the same collected radiation:

$$P_{coll} \propto VI = P_{in}^{elect} = P_{in}^{beam} \tag{14}$$

While the electric power is distributed all over the filament,the beam power is deposited in a zone delimited by beam width. Due to the thinness of filaments the incident flux F perpendicular to the wire can be considered constant. It hits only half surface:

$$\int_{S_{eff}} F dx dy = 2rFL \tag{15}$$

The total area of the filament in which the beamlet group deposits power is $2rL$, where L is beam width. This yields that $P_{in}^{beam} = 2rLF$ and so $\frac{VI}{2rL} = F$. On the other hand, heated filaments emit in all directions, as visible in figure 20 ; after naming q_{irr} the emitted light flux, at the equilibrium:

$$q_{irr} 2\pi r L = VI \tag{16}$$

Thus yields:

$$q_{irr} = \frac{F}{\pi} \tag{17}$$

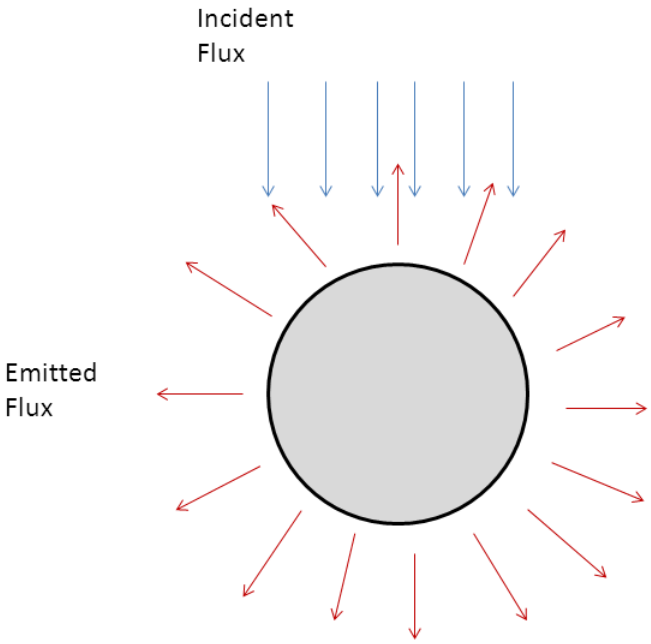

Figure 20: Sketch of direction of F and q_{irr}

3.3.3 Spectrometer

To resolve uncertainties about temperature values a spectrometer was used to collect filament spectrum. This tool collects electromagnetic radiation,through a 1:1000 filter, between $300nm$ and $850nm$. Collected spectra have to be recalibrated due to several effects caused by spectrometer electronic or filter used to avoid saturation. However, the curve of the calibration lamp was not complete as it stopped at $800nm$,but as can be seen in Figure 21,it can be described by a Planck's curve; therefore, a theorical reconstruction can be done. Temperature of this lamp can be obtained after the fit to these data. Then the curve has been expanded until it reached $850nm$. This allows to use and extend wavelength interval.

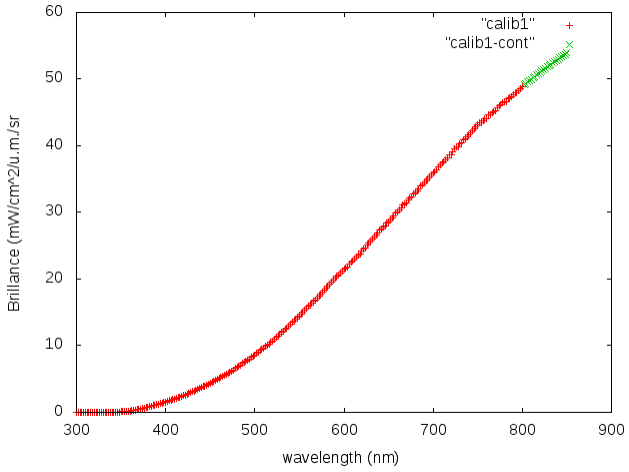

Figure 21: Calibration lamp curve. In red, the original curve, in green the estimated part used for expansion

A new calibration file was created and it was applied to the experimental collected spectra 22. An example of results dis given in figures 23a and 23b.

Data have been fitted to extrapolate the temperature values and also to try to determine the temperature dependence of emissivity. Due to the difficulty to fitting Planck's curve, it has been necessary to perform some data computation to obtain a linear fit. As described in Equation 8, $B(\nu)d\lambda = \frac{2\gamma hc^2\epsilon}{\lambda^5}\frac{1}{e^{\frac{hc}{kT\lambda}}-1}d\lambda$, where γ is a parameter, representing geometric constants and solid angles.

Since $1000K < T < 3000K$ and $300 \cdot 10^{-9}nm < \lambda < 850 \cdot 10^{-9}nm$, $\frac{hc}{\lambda Tk} \gg 0$, the following approximation can be adopted:

$$B(\lambda)\frac{\lambda^5}{2hc^2} = \frac{1}{e^{\frac{hc}{kT\lambda}}-1} \approx \frac{1}{e^{\frac{hc}{kT\lambda}}} \tag{18}$$

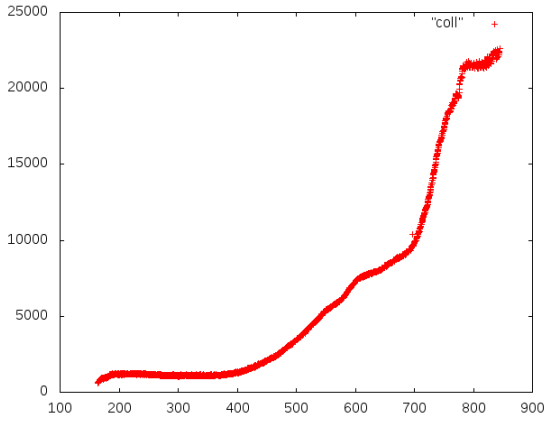

Figure 22: Collected spectra

where B(λ) are the experimental data and have arbitrary unit (a.u.). Upon defining

$\gamma \cdot \epsilon = \alpha$

$$-\frac{hc}{kT\lambda} + ln(\alpha) = ln\left(\frac{\lambda^5 I(\lambda)}{2hc^2}\right) \tag{19}$$

Plotting $(\frac{1}{\lambda}, ln\left(\frac{\lambda^5 I(\lambda)}{2hc^2}\right))$ a linear fit is obtained.

Defining $A = ln(\alpha)$ and $B = \frac{hc}{kT \cdot 10^{-6}}$, the equation becomes:

$$y = A + Bx \tag{20}$$

Considering that $\gamma \cdot \epsilon = \alpha$, the emissivity trend can be obtained. Upon assuming that γ is equal for all data of the same experimental set, and defining α_{max} as the maximum value of α of the same set, the ratio:

$$\frac{\alpha_i}{\alpha_{max}} = \frac{\epsilon_i}{\epsilon_{max}} \tag{21}$$

Plotting $(T_i\ ,\ \frac{\epsilon_i(T_i)}{\epsilon_{max}(T)})$ and fitting it with a generic function such as:

$$y = ax^b + c \tag{22}$$

it is possible to find the temperature dependency of the emissivity. This analysis has been realized only for the last experimental set and some fit examples are reported in Figures 23 and 24.

All these fits have been done with all collected spectra: T and α pairs are reported in Tables 6, 7 (appendix) and in figures 25a, 25b.

All fits have been performed by "cutting" lower wavelengths, affected by larger errors, until the obtained curve fits quite well the upper part of data plot. It has been

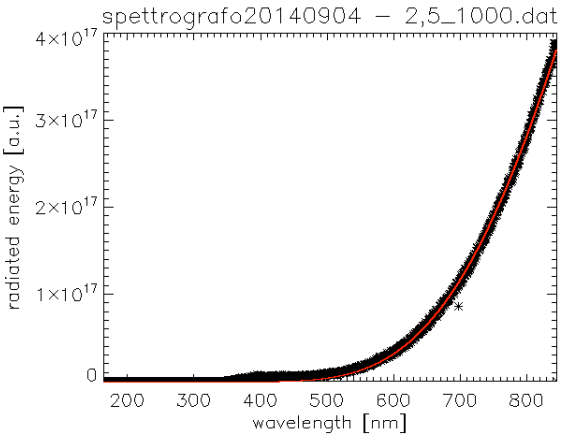

(a) Filament 0.2mm, 2.5A

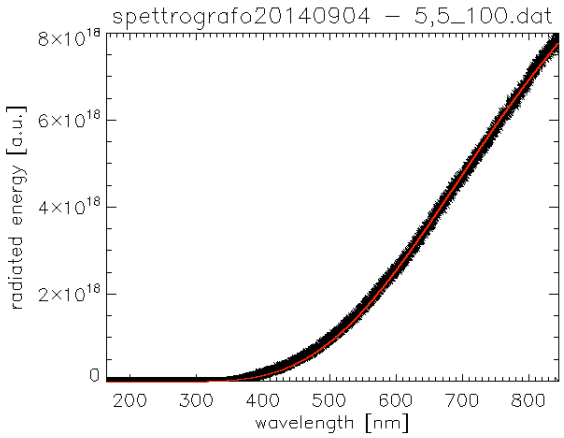

(b) Filament 0.2mm, 5.5A

Figure 23: Fit spectra

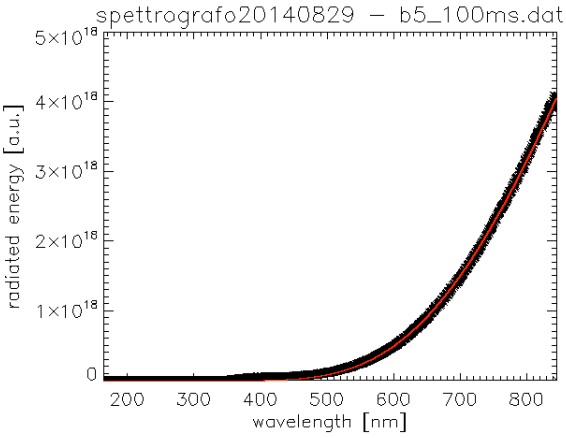

(a) Filament 0.3mm, 5A, second session

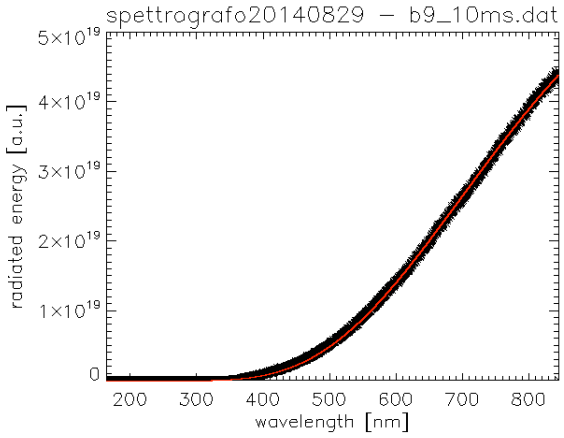

(b) Filament 0.3mm, 9A, second session

Figure 24: Fit spectra

seen that even a little modification of the data window causes non-negligible differences on α, while big differences have not been seen on temperature values.

An estimation of $\alpha(T)$ can be done: filament 7 and 8 yields different (T , α) behaviour, as can be in the following figures. In Figure 25a there is no recognizable trend. In Figure 25b two different clear trends are visible: in the first part, α decreases with increasing temperature, while in the second part it increases. No explanation has been found, but probably some problems on the spectrometer have occured. An independent estimation of the effect of temperature on emissivity has been carried out and the results suggest a non-dependency of α on temperature[17].

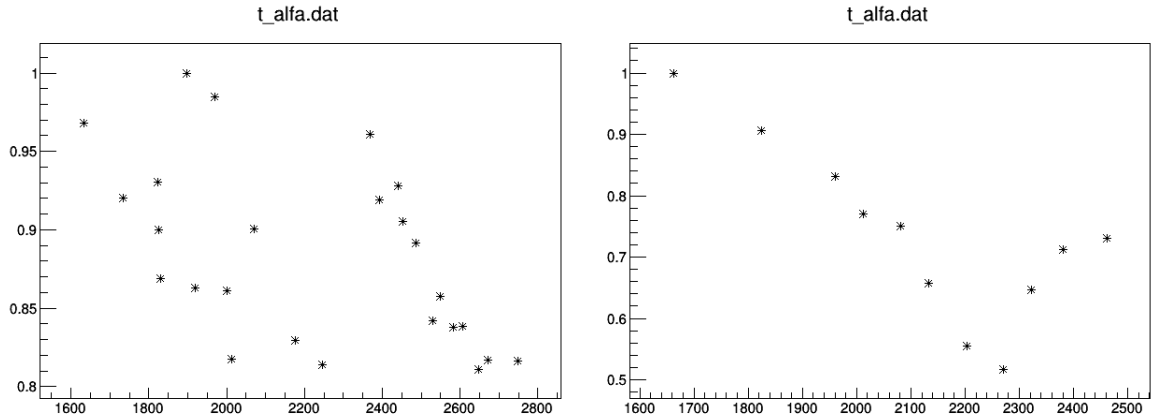

(a) Filament 0.3mm

(b) Filament 0.2mm

Figure 25: (T,α) couples of the two experimental set analized with the spectrometer. Two different trends can be istantly recognized. Data tables are reported in the appendix: tables 7 and 6.

These new temperature values can be plotted with P_{coll} (figure 26). It can be seen that he slope of the experimental data is higher than for theoretical computations, which is the opposite with respect to figure 17.

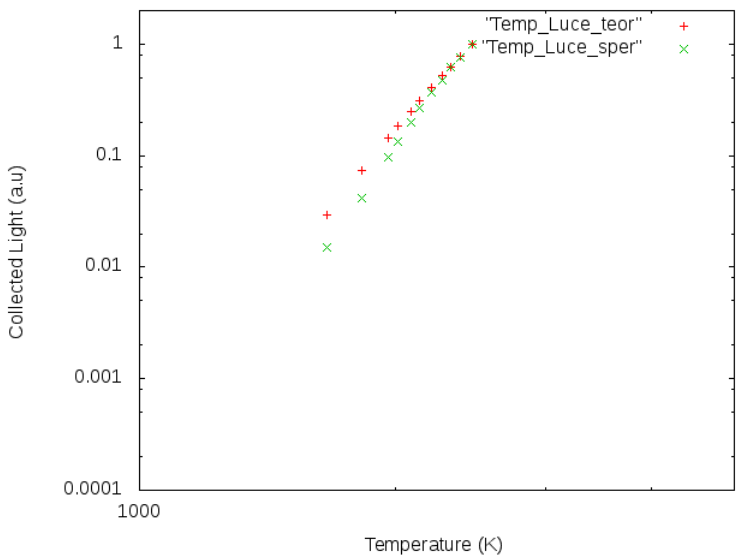

Figure 26: Bilogarithmic plot of (T ; P_{coll})

Moreover, using these temperatures a correction to equation (12) is possible: by inverting it, the filament length can be obtained and can be used in analysis. In tables 4 and 5 these values are reported along with the temperature estimated by the spectrometer data. The resulting values of the effective length vary with temperature, which is anyway consistent with the visual observations reported in section 3.3.2. It is found that the effective length can result larger than the measured length of the wire (225 mm). In the search for possible explanations, several hypotheses can be considered. The determination of the effective length (equation 12) depends on the wire cross-section, so the effect of a small uncertainty in the wire diameter is checked. A 5% reduction of the tungsten wire diameter yields a reduction of the effective length (see column 4 of tables 4 and 5), though the problem is not solved yet, so that a further 7% higher temperature should be invoked. Considering all the experimental error sources involved in temperature estimate from the spectrometer, this discrepancy could be marginally comprised within experimental uncertainty.

It has to been noted that the two filaments broke at about $2500K$ and $2800K$. Those temperatures are lower than expected, but breakdown was probably caused by mechanical stresses due to thermal expansion of filaments and by the softening which occurs well before melting temperature.

$T(K)$	$I(A)$	$l^*(m)$	$l'^*(m)$
2461	5.5	0.284	0.256
2381	5.2	0.272	0.245
2322	5.0	0.272	0.246
2270	4.7	0.267	0.241
2203	4.5	0.265	0.240
2134	4.2	0.264	0.239
2082	4.0	0.258	0.233
2012	3.7	0.252	0.227
1960	3.5	0.247	0.223
1825	3.0	0.238	0.215
1662	2.5	0.232	0.209

Table 4: Effective length, filament 9

$T(K)$	$I(A)$	$l^*(m)$	$l'^*(m)$
1826	5	0.236	0.213
1918	5.5	0.239	0.216
2001	6	0.243	0.220
2071	6.5	0.247	0.222
2246	7.5	0.252	0.227
2394	8.6	0.264	0.239
2440	9	0.266	0.240
1632	4	0.232	0.210
1735	4.5	0.234	0.212
1824	5	0.240	0.217
1898	5.5	0.246	0.222
1971	6	0.246	0.222
2368	8.5	0.266	0.240
2606	10	0.271	0.244
2649	10.2	0.273	0.246
2671	10.4	0.274	0.248
2729	11	0.275	0.248
2747	11.2	0.276	0.249
1830	5	0.234	0.211
2013	6	0.242	0.218
2177	7.5	0.262	0.236
2452	9	0.267	0.241
2486	9.2	0.268	0.242
2530	9.4	0.268	0.241
2550	9.6	0.270	0.243
2583	9.8	0.270	0.244

Table 5: Effective length, filament 8

4 Numerical simulations and comparison with ELISE data

Simulations will provide fundamental information about filament temperature, emitted radiation, temperature gradient. A simulation with COMSOL Multiphysics 3.5 software, based on finite element method, has been performed to simulate the incident beam on the wire calorimeter. Finite element method is a numerical technique used to find approximated solutions to boundary value problems for partial differential equations. One dimensional model has been selected as the filament has a more little section than the filament profile and it can be considered as a segment.

The total power,equal to $141kW$, was estimated using equation 4 and keeping the perveance constant. Power is deposited by 640 beamlets, distributed into 8 beamleat group, each one composed of 5×16 beamlets, as described in section 1.3. To perform simulations, the same parameters of the experimental device has been used, to have results as realistic as possible. Distance D_{GC} between the Ground Grid and the calorimeter is $1.8m$, diameter wires is $0.2mm$.

Beamlet beam can be describes as a gaussian function[2]centered in different positions on the wire. Divergence was considered as $\delta = 2°, 3°, 4°$.

The resolved equation is:

$$\delta\rho C_p \frac{\partial T}{\partial t} - \nabla(k\nabla T) = Q + C_t(T_{amb}^4 - T^4) \tag{23}$$

where $C_t(T_{amb}^4 - T^4)$ represents the emitted radiation power per unit volume, Q is the power per unit volume of incident beamlets, $\nabla(k\nabla T)$ is power per unit volume conducted along the wire, k the thermal conductivity, ρ tungsten density and C_p the specific heat at constant pressure.

Two different cases has been simulated:

- Using only horizontal beamlets (divided into 4 groups)
- Using only vertical beamlets (divided into 2 groups)

Horizontal and vertical wires have the same length ($1.5m$).

Simulations consider $10s$, divided into step of 0.015

The model is based on the conservation of the heat sources and parameters of equation 23 have to be supplied. The energy flux deposited by the beam F have to be input to simulations as a generation of energy per unit volume. The energy flux is integrated over the surface heated by the beam $(2rl)$ and divided by the volume $(\pi r^2 l)$. The resulting equation is:

$$Q = F\frac{2rl}{\pi r^2 l} = \frac{2F}{\pi r} \tag{24}$$

[2]gaussian 1-D function: $\frac{1}{\sqrt{\pi}\sigma} e^{-\frac{(x-x_0)^2}{\sigma^2}}$

Considering the C_t constant:

$$C_t(T_{amb}^4 - T^4) = \epsilon\sigma\frac{2\pi rl}{\pi r^2 l}(T_{amb}^4 - T^4) \tag{25}$$

and

$$C_t = \frac{2\epsilon\sigma}{r} \tag{26}$$

In the simulation, due to the large beamlet divergence, the superposition of the effect of several beamlets was considered using a simplifying hypothesis: 6 columns and 16 rows of sorrounding beamlets were added together by multiplying a constant K to the total input power.

Considering the gaussian form of beams,

$$K = \sum_{i=1}^{6}\sum_{j=1}^{16} e^{-\frac{(\Delta x_{i,j})^2+(\Delta y_{i,j})^2}{\sigma_i^2}} \tag{27}$$

where $\sigma_i \approx D_{GC} \cdot \delta$, Δx is the distance between the central beamlet column and the others and $\Delta y$the distance between the central beamlet row and the others . Following values were found: $K(\delta = 2°) = 16.27$, $K(\delta = 3°) = 28.13$, $K(\delta = 4°) = 33.35$.

In figure27 a simulation is shown. In particular, effects of each beamleat group are visible.

In figure 28 a comparison between horizontal and vertical wire is are shown.

In figure 29 horizontal simulation with different divergence are shown:the larger the beam divergence, the less the single beamlet groups can be distinguished (figures 29). Considering figure 5 a qualitative comparison between these simulations and ELISE images can be performed. These simulations show that, after a suitable calibration, a tungsten wire calorimeter can be used to deduce quantitative data about the two-dimensional pattern of the beam energy flux. .

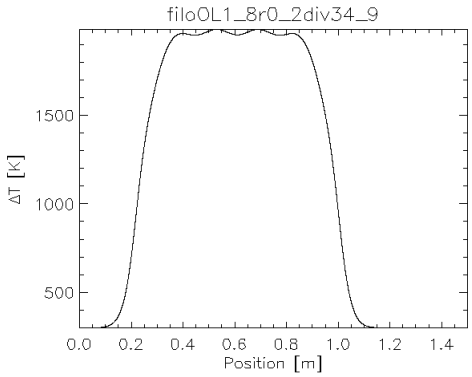

(a)

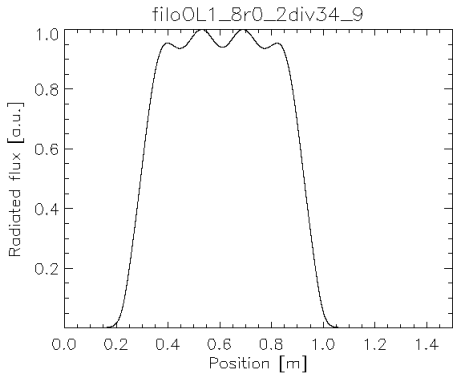

(b)

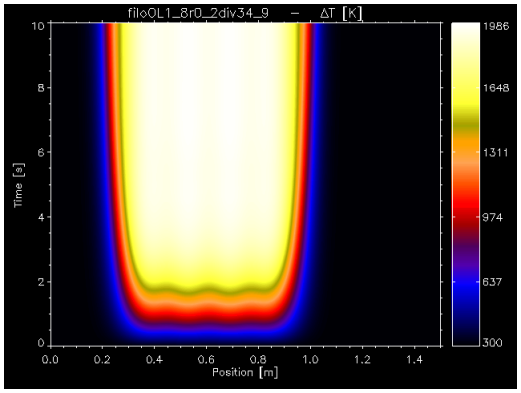

(c)

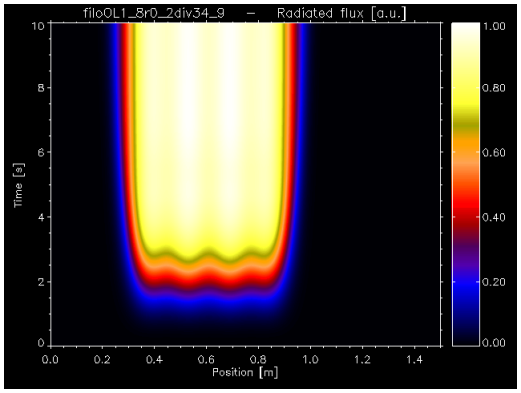

(d)

Figure 27: Horizontal simulation, $\delta = 2°$: Images a) and b) represent respectively temperature of the filament and radiative flux along the filament. Images c) and d) represent respectively temperature and radiative flux as a function of time and position.

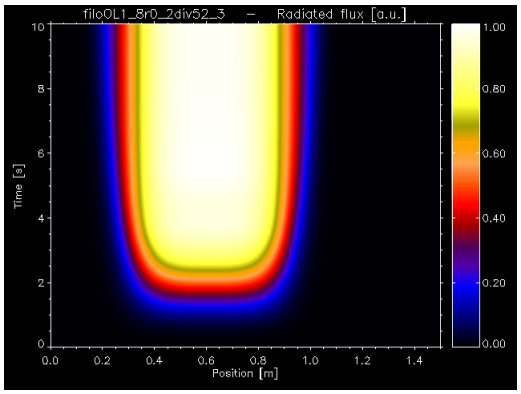

(a)

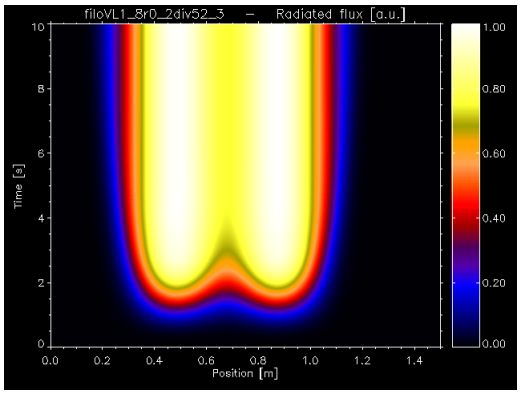

(b)

Figure 28: $\delta = 3°$, horizontal and vertical radiative fluxes

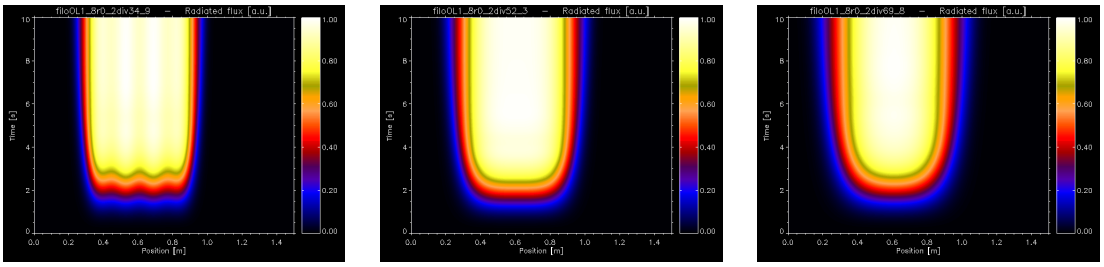

(a) (b) (c)

Figure 29: Radiative flux as a function of beam divergence. a) corresponds to the case of $\delta = 2°$, b) to the case of $\delta = 3°$ and c) $\delta = 4°$.

Conclusions

Optimization of ITER Neutral Beam Injectors requires the accurate measurement of beam parameters. The work presented in this thesis demonstrates that a tungsten wire calorimeter of the type used at IPP in the facilities BATMAN and ELISE can be used to obtain quantitative data about the energy flux associated to particle beams.

An experiment was setup involving tungsten filaments placed in vacuum chamber, which have been ohmically heated to study their behaviour and light emission and simulations were performed to estimate the heating of filaments subjected to energy flux.

In the first part of the work, the experiment was designed: in particular, copper supports for the filaments have been designed and built during this thesis.
During the experiments data have been collected using several filaments of different diameters. A CCD camera was used to collect images of heated filaments, while a spectrometer was employed to measure emission spectrum.
Finally it has been demonstred that, after a proper electrical calibration, tungsten filaments can be used to obtain quantitative data about particle beams since input power and collected power have a monotonic relationship. Equations 16 and 17 also yield the relation between beam energy flux and emitted light flux.

Emission spectra collected with spectrometer allows the calculation of filament temperatures that also yields a parameter for the determination of the effective filament length.
With this tool the emissivity as a function of the temperature was studied, without reaching conclusive results, so that a constant value has been assumed.

Simulations performed on 1-D filaments reproduce the main features of ELISE wire calorimeter; a quantitative comparison is not possible as so far this calorimeter was only used to obtain beam profile images.

In future, NIO facility, developed at Consorzio RFX, could be used to test in a more realistic situation the potentiality of a tungsten wire calorimeter, before using it on SPIDER.

Appendix

In this appendix tables about graphs 25a and 25b are reported.

filename	alpha (a.u).	sigma_alpha(a.u.)	temperature (K)	sigma_temperature (K)
5,5_100.dat	2.86488e+07	1.19601e+05	2.46087e+03	1.23160e+00
5,2_100.dat	2.79394e+07	1.18664e+05	2.38094e+03	1.17709e+00
5_100.dat	2.53822e+07	1.08568e+05	2.32228e+03	1.12440e+00
4,7_300.dat	2.03054e+07	7.78682e+04	2.27035e+03	9.49354e-01
4,5_300.dat	2.17968e+07	8.55919e+04	2.20273e+03	9.31757e-01
4,2_300.dat	2.57837e+07	1.08352e+05	2.13359e+03	9.43534e-01
4_300.dat	2.94089e+07	1.19025e+05	2.08186e+03	8.57324e-01
3,7_500.dat	3.02268e+07	1.21298e+05	2.01231e+03	7.94204e-01
3,5_700.dat	3.26204e+07	1.40847e+05	1.95988e+03	8.25623e-01
3_1000.dat	3.55524e+07	1.59412e+05	1.82482e+03	7.29754e-01
2,5_1000.dat	3.92305e+07	3.80395e+05	1.66196e+03	1.34165e+00

Table 6: Data table, graph 25b

filename	alpha (a.u).	sigma_alpha(a.u.)	temperature (K)	sigma_temperature (K)
b5,5_100ms.dat	1.91846e+03	6.89968e-01	1.59327e+08	6.42617e+05
b5_100ms.dat	1.82594e+03	7.74066e-01	1.66114e+08	8.19174e+05
b6,5_50ms.dat	2.07141e+03	6.37553e-01	1.66198e+08	5.30281e+05
b6_100ms.dat	2.00112e+03	5.98090e-01	1.58988e+08	5.00099e+05
b7,5_50ms.dat	2.24626e+03	6.35457e-01	1.50252e+08	4.12507e+05
b8,6_10ms.dat	2.39372e+03	8.85414e-01	1.69673e+08	5.59926e+05
b9_10ms.dat	2.44045e+03	1.01731e+00	1.71285e+08	6.05655e+05
c4,5_100ms.dat	1.73471e+03	8.29674e-01	1.69837e+08	9.63234e+05
c4_300ms.dat	1.63209e+03	6.61918e-01	1.78691e+08	9.05570e+05
c5,5_50ms.dat	1.89772e+03	7.40783e-01	1.84609e+08	7.79037e+05
c5_100ms.dat	1.82434e+03	7.03246e-01	1.71770e+08	7.44598e+05
c6_50ms.dat	1.97082e+03	7.14174e-01	1.81784e+08	6.79663e+05
c8,5_10ms.dat	2.36776e+03	1.01078e+00	1.77438e+08	6.56501e+05
d10,2_10ms.dat	2.64872e+03	9.96145e-01	1.49754e+08	4.60321e+05
d10,4_10ms.dat	2.67069e+03	1.18149e+00	1.50801e+08	5.26088e+05
d10_10ms.dat	2.60600e+03	1.10338e+00	1.54747e+08	5.29503e+05
d11,2_10ms.dat	2.74726e+03	1.41163e+00	1.50640e+08	5.76130e+05
d11,4_10ms.dat	2.76875e+03	1.51103e+00	1.46546e+08	5.96151e+05
d11,6_10ms.dat	2.80731e+03	1.45805e+00	1.40674e+08	5.48124e+05
d11_10ms.dat	2.72857e+03	1.37391e+00	1.50628e+08	5.72139e+05
d12,2_10ms.dat	2.81960e+03	1.69827e+00	1.38874e+08	6.15979e+05
d12,4_10ms.dat	2.04562e+03	1.30744e+01	3.24560e+09	2.93465e+08
d12,4_10ms.dat	2.83859e+03	1.47519e+00	1.34276e+08	5.25001e+05
d12_10ms.dat	2.80062e+03	1.60395e+00	1.44823e+08	6.05947e+05
d5_100ms.dat	1.82986e+03	7.42933e-01	1.60397e+08	7.43047e+05
d6_100ms.dat	2.01255e+03	6.26168e-01	1.50873e+08	4.92150e+05
d7_50ms.dat	2.17748e+03	6.64161e-01	1.53115e+08	4.57888e+05
d9,2_10ms.dat	2.48568e+03	1.03247e+00	1.64583e+08	5.72106e+05
d9,4_10ms.dat	2.52983e+03	8.56465e-01	1.55456e+08	4.56390e+05
d9,6_10ms.dat	2.54969e+03	1.04766e+00	1.58336e+08	5.37399e+05
d9,8_10ms.dat	2.58291e+03	1.00305e+00	1.54679e+08	4.96810e+05
d9_10ms.dat	2.45233e+03	1.00003e+00	1.67117e+08	5.77543e+05

Table 7: Data table, graph 25a

References

[1] M. Kikuchi, K. Lackner, and Q. M. Tran, eds *Fusion Physics* IAEA International Atomic Energy Agency.

[2] ITER website *www.iter.org*

[3] J. D. Callen, *Fundamentals of Plasma Physics*, University of Winsconsin, Madison (2003)

[4] H. P. L. de Esch et al., *The optimization of neutral beams for ignition and burn control on next-step reactors*, Fusion Eng. and Des. 26, 589-604 (1995)

[5] Max-Planck Institut für Plasmaphysik, *Official website, www.ipp.mpg.de*

[6] I. G. Brown,*The Physics and Technology of Ion Sources*, WILEY-VCH Verlag GmbH & Co. KGaA, Weinheim (2003)

[7] P. Sonato et al. *Status of PRIMA, the test facility for ITER neutral beam injectors* AIP Conf. Proc. 1515 (2013), p. 549.

[8] P. Sonato et al. , *The ITER full size plasma source device design*: Fusion Enginnering and Design (2009)

[9] B. Heinemann et al., *Design of the "half-size" ITER neutral beam source for the test facility ELISE*, Fusion Eng. Des. 84, 915-922 (2009)

[10] P. Strehl, *Beam Instrumentation and Diagnostics*,Springer, Berlin (2006)

[11] Riccardo Nocentini et al. , *Beam diagnostic tools for the negative hydrogen ion source test facility ELISE*: Fusion Eng. Des. 88 (2013) 913

[12] P. Franzen et al., *Progress of the ELISE Test Facility: Results of Cesium Operation with low RF Power, submitted to Nucl. Fusion*

[13] Marcello Carlà *Stefan-Boltzmann law for the tungsten filament of a light bulb: Revisitin the experiment*: Am.J.Phys. 81, pages 512-517 (2013)

[14] B.S.N. Prasad & Rita Mascarenhas *A laboratory experiment on the application of Stefan's law to tungsten filament electric lamps*: Am.J.Phys. 46, pages 420-423 (1978)

[15] Forsythe and Worthing, *The properties of tungsten and the characteristics of tungsten lamps*, The Astrophysical Journal (1934)

[16] Forsythe and Watson, *Resistance and Radiation of Tungsten as a Function of Temperature* ,J.O.S.A. 24 (Apr. 1934).

[17] Isabella Mario, *Feasibility study of a diagnostic wire calorimeter for the SPIDER experiment* Bachelor Thesis, Università degli Studi di Padova

[18] F. J. Abellan et al, *The Stefan-Boltzmann constant obtained from the I-V curve of a bulb* European Journal of Physics 34 (2013)

[19] K. opto-electronics GmbH. *SDK4 for Zelos cameras. url: www.kappa.de.*